DYNAMIC PHOTOPHYSIOLOGICAL STRESS RESPONSE OF A MODEL DIATOM TO TEN ENVIRONMENTAL STRESSES[1]

Zhengke Li [ID][2]

Department of Oceanography, Dalhousie University, 1355 Oxford St, Halifax, NS B3H 4R2, Canada

Wei Li

College of Life and Environmental Sciences, Huangshan University, Huangshan 245041, China

Yong Zhang

College of Environmental Science and Engineering, Fujian Normal University, Fujian 350007, China

Yingyu Hu

Department of Oceanography, Dalhousie University, 1355 Oxford St, Halifax, NS B3H 4R2, Canada

Rosie Sheward

Institute of Geosciences, Goethe-University Frankfurt, Frankfurt am Main 60438, Germany

Andrew J. Irwin [ID]

Department of Mathematics & Statistics, Dalhousie University, 1355 Oxford St, Halifax, NS B3H 4R2, Canada

and Zoe V. Finkel [ID]

Department of Oceanography, Dalhousie University, 1355 Oxford St, Halifax, NS B3H 4R2, Canada

Stressful environmental conditions can induce many different acclimation mechanisms in marine phytoplankton, resulting in a range of changes in their photophysiology. Here we characterize the common photophysiological stress response of the model diatom *Thalassiosira pseudonana* to ten environmental stressors and identify diagnostic responses to particular stressors. We quantify the magnitude and temporal trajectory of physiological parameters including the functional absorption cross-section of PSII (σ_{PSII}), quantum efficiency of PSII, non-photochemical quenching (NPQ), cell volume, Chl *a*, and carotenoid (Car) content in response to nutrient starvation (nitrogen (N), phosphorus (P), silicon (Si), and iron (Fe)), changes in temperature, irradiance, pH, and reactive oxygen species (ROS) over 5 time points (0, 2, 6, 24, 72 h). We find changes in conditions: temperature, irradiance, and ROS, often result in the most rapid changes in photophysiological parameters (<2 h), and in some cases are followed by recovery. In contrast, nutrient starvation (N, P, Si, Fe) often has slower (6-72 h) but ultimately larger magnitude effects on many photophysiological parameters. Diagnostic changes include large increases in cell volume under Si-starvation, very large increases in NPQ under P-starvation, and large decreases in the σ_{PSII} under high light. The ultimate goal of this analysis is to facilitate and enhance the interpretation of fluorescence data and our understanding of phytoplankton photophysiology from laboratory and field studies.

Key index words: diatom; environmental stress; fluorescence; stress response; *Thalassiosira pseudonana*

Abbreviations: Car, carotenoids; F_v/F_m, the maximum quantum yield of PSII photochemistry; NPQ, non-photochemical quenching; ROS, reactive oxygen species; σ_{PSII}, the functional absorption cross-section of PSII; Φ_{PSII}, the PSII operating efficiency under actinic light

Diatoms are among the most successful phytoplankton groups, responsible for a large proportion of total marine primary production and carbon export (Field et al. 1998, Tréguer et al. 2018). The ocean is highly dynamic with rapid changes in environmental conditions, including temperature, light, pH, and the availability of key nutrients. Diatoms respond to shifts in these conditions by altering their physiological state, resulting in changes to community composition and productivity. The ability of diatoms to acclimate to rapidly changing environmental conditions is likely a key factor in their

ecological success (De La Rocha and Passow 2004, Armbrust 2009).

Chlorophyll fluorescence parameters and pigment content are frequently used to assess physiological status, identify dominant environmental stressors, and quantify phytoplankton biomass and productivity in situ and in laboratory studies (Boyd and Abraham 2001, Young and Beardall 2003, Gorbunov and Falkowski 2005, Behrenfeld et al. 2006, Moore et al. 2006, Prasil et al. 2008, Suggett et al. 2009). These parameters provide insight into photochemical processes associated with light harvesting and processes facilitating carbon fixation and can quantify the balance between energy absorbed through photochemistry and energy-demanding metabolic processes under environmental stresses (Huner et al. 1998, Wilson et al. 2006, Kramer and Evans 2011). For example, the functional absorption cross-section of PSII (σ_{PSII}) enables an estimate of light absorbed by the PSII apparatus. F_v/F_m and PSII operating efficiency under actinic light (Φ_{PSII}) provide estimates of the quantum efficiency of PSII after dark-adaptation and under actinic light, respectively. Non-photochemical quenching (NPQ) of the PSII antenna provides an estimate of the thermal dissipation of excess excitation energy absorbed by the cell. Much experimental work has been conducted to quantify the photophysiology of phytoplankton in response to single environmental factors in an attempt to identify photophysiological markers of particular environmental stressors (e.g., Parkhill et al. 2001, Young and Beardall 2003). Some work has also been conducted to test how phytoplankton respond to multiple environmental drivers (Brennan and Collins 2015, Boyd et al. 2018, Li et al. 2018, Gao et al. 2019). Despite these efforts, still more work is required to be able to distinguish the effects of different environmental stressors and interpret these parameters under dynamic conditions in the field.

To make sense of photophysiological responses under non-steady-state conditions, the experimenter must describe the nature of the perturbation and the time between the change in the environment and the fluorescence observation. Although we know that the up-regulation of NPQ and changes in PSII quantum yield can be very fast (Kolber et al. 1998), many of the published observations in nutrient-starved conditions are made 24-48 h following perturbation (Geider et al. 1993, Liu et al. 2011, Liefer et al. 2018). Experimental work to date has not used a consistent species/strain/ecotype with similar physiological status and lacks a standard experimental design and timing for assaying photophysiology in response to non-steady-state stressors. There are a very large number of possible experiments, which makes comparison across studies and labs difficult. For example, it is difficult to compare the photophysiological response of *Phaeodactylum tricornutum* to nitrogen or phosphorus starvation from previous studies due to differences in sampling and culture conditions used by different investigators (Geider et al. 1993, Abida et al. 2015, Alipanah et al. 2015, 2018). As a result, both the time required to get a significant change in a specific photophysiological parameter and the relative magnitude of the change in response to a variety of different environmental stressors are not well described in the literature.

Here we hypothesize that environmental stressors will cause similar photophysiological responses if they cause a similar imbalance between light energy absorbed and metabolic demand, reactive oxygen generation and damage. To test this hypothesis we investigated the dynamic photophysiological responses of the model diatom *Thalassiosira pseudonana* to 10 common environmental perturbations, including 5 environmental conditions (2 irradiances, 2 temperature treatments, lowered pH), starvation to 4 different mineral resources (nitrate, phosphate, iron, and silicic acid), and elevated H_2O_2 (used as a positive control because ROS levels are expected to increase under many stressors) at 5 time points over 72 h. Environmental stressors can impact photophysiology directly, including by damage, and indirectly by remodelling and recovery. All stressors have the potential to stimulate an imbalance between the light energy absorbed through photochemistry versus the energy needed to fuel metabolism (Demmig-Adams and Adams 1992, Huner et al. 1998, Hughes et al. 2018) and therefore may show some similarity in response due to the over-excitation of PSII and photo-oxidative stress. We also expected some differences in the magnitude and timing of the effect on various photophysiological parameters across different types of stressors, in particular those that lead to a surplus versus a deficit in photons absorbed compared to the energy demand to fuel metabolism. Our systematic study of one diatom species under otherwise identical laboratory conditions illuminates the contrasts in photophysiological response, including changes in fluorescence parameters and changes in cell volume, Chl *a*, and carotenoid content, across a wide range of stressors over time, and thus facilitates the identification of common and unique photophysiolgical responses to different environmental stressors.

MATERIALS AND METHODS

Strain and culture conditions. The coastal diatom *Thalassiosira pseudonana* (CCMP 1335) was obtained from the Bigelow National Center for Marine Algae and Microbiota (formerly CCMP). Axenic clones were purified by streaking diluted liquid culture on agar plates. The following experiments were conducted on cultures derived from a single clone. Cultures were maintained in 250 mL polycarbonate bottles (Nalgene, USA) with 250 mL modified ESAW medium (Berges et al. 2001, see Media preparation section). Continuous illumination was provided by LED bulbs. Irradiance was monitored using Biospherical Instruments QSL 2101.

Temperature was maintained using growth chambers (Conviron A1000, Conviron, Manitoba, Canada). Cultures were manually agitated four to five times each day in order to reduce cell sedimentation. Under our growth conditions, the optimal growth temperature for *T. pseudonana* was 23°C and saturating growth irradiance was 200 µmol photons · m^{-2} · s^{-1}.

Experiment design. Ten stress conditions plus a control condition were evaluated in this study (Table 1), including 4 nutrient starvation treatments (a transfer of cells into N-, P-, Si-, and Fe-free media); an elevated (26°C) and a depressed temperature (14°C) treatment relative to the control maintained at 20°C; a low-light (10 µmol photons · m^{-2} · s^{-1}) and high-light treatment (800 µmol photons · m^{-2} · s^{-1}) relative to the control maintained at 100 µmol photons · m^{-2} · s^{-1}; a low-pH treatment (pH 7.8) relative to the control maintained at pH 8.1; and a reactive oxygen species (ROS) stress treatment that was created by exogenous addition of 0.165 mM H$_2$O$_2$. The control allows us to account for the impact of handling and separate it from the impact of the environmental treatments on the physiological parameters. Extensive preliminary experiments were conducted to choose our temperature, light, and H$_2$O$_2$ treatments. We chose 14°C as our low-temperature treatment and 10 µmol photons · m^{-2} · s^{-1} as our low-light treatment based on preliminary experimental work that indicated these values would lower growth rates to between half to one-third of that achieved under 20°C and 100 µmol photons · m^{-2} · s^{-1}. The high-temperature treatment (26°C) and the high-light treatment (800 µmol photons · m^{-2} · s^{-1}) were selected to trigger a high-temperature response and a high-light response without a detectable influence on division rate. Preliminary experimental work identified H$_2$O$_2$ concentration ≤ 0.15 mM as a non-lethal but detectable ROS treatment. Taking into consideration the degradation of H$_2$O$_2$ after opening the original bottle, we increased the H$_2$O$_2$ concentration to 0.165 mM. Cultures exposed to H$_2$O$_2$ exhibited immediate detectable photophysiological responses, followed by recovery over the 72 h of the experiment.

Samples were taken at 5 time points: 0 (initiation of the treatment), 2, 6, 24, and 72 h after the initiation of the treatment. Four independent biological replicates of each treatment were run and assayed. To maintain stable conditions, each sample was taken from a separate bottle (each treatment and time point had 4 replicate bottles). Cells at all conditions and all time points were sampled at a final cell concentration of 5×10^5 cells · mL^{-1}. A series of pre-experiments for each experimental treatment was conducted to determine the ideal cell density to initiate the experiment and for sampling. Stock cultures for each condition were acclimated for over 20 generations in the mid-exponential phase under the control conditions before the treatment. Stock cultures were then filtered onto polycarbonate (PC) Millipore membranes (pore size: 0.8 µm, diameter: 47 mm) and washed three times with ESAW media modified according to treatment (N-, P-, Si-, Fe-free for nutrient starvation; pH 7.8 for low-pH stock cultures, pH 8.1 for other treatments), followed by suspending cells in the same modified ESAW media. Suspended cells were counted and transferred to the prepared and acclimated media in 250 mL PC bottles. Pre-experimental work found that pH varied < 0.05 over the experiment over the planned range of cell concentrations. Cell concentrations and cell volume were monitored at each sampling point using a Z2 Coulter Counter (Beckman Coulter) with Coulter Z2 AccuComp software. We initiated each culture with a different cell density, chosen using pre-experiments to achieve a desired cell density at the sampling time. As a result, the observed cell density, $X(t)$, for each bottle was approximately 5×10^5 cells · mL^{-1} at the 4 sampling times ($t > 0$). To determine the trajectory of increase in cell density over the time course of each treatment, we computed the cell density scaled by initial density on a log scale, $\ln (X(t)/X(0))$, for each bottle at its sampling time. This quantity measures the amount of growth in each bottle, quantified as the ratio of cell density at the sampling time relative to the initial cell density. Because growth is exponential, we log transform this and refer to the resulting parameter as *accumulated growth*. For the control bottles, the function is a straight line reflecting balanced growth. To facilitate comparisons across treatments, we normalize the accumulated growth parameter at time t by the *accumulated growth* in the control and refer to it as *relative accumulated growth*.

Media preparation. ESAW media was set to pH 7.8 (low-pH) or pH 8.1 (control and all other treatments) using 16 mM N-(2- hydroxyethyl)-piperazine-N9-2-propanesulfonic acid (EPPS; Sigma-Aldrich), adjusted with ultra-pure HCl/NaOH. Media was filtered through 0.2 µm Whatman POLYCAP filters and supplemented with 0.22 µm-filtered vitamins and inorganic nutrients. The nutrient-replete treatments and controls had final concentrations of 100 µM NaNO$_3$, 20 µM Na$_2$PO$_4$, 150 µM Na$_2$SiO$_3$·9H$_2$O, and 6.56 µM Fe with a Na$_2$EDTA concentration of 100 µM. The N-, P-, and Si-starvation treatments were made by adding rinsed cells to media with no addition of NaNO$_3$, Na$_2$PO$_4$, and Na$_2$SiO$_3$·9H$_2$O, respectively. The iron stock was made with an Fe-EDTA solution of FeCl$_3$·6H$_2$O (CAS No. 10025-77-1, Sigma-Aldrich Inc.) with 100 µM Na$_2$EDTA. The iron-free treatment had a final Na$_2$EDTA concentration of 100 µM (no FeCl$_3$·6H$_2$O addition). For the hydrogen peroxide (H$_2$O$_2$) treatment, a final H$_2$O$_2$ (Sigma) concentration of 0.165 mM was achieved in the acclimated ESAW media before the cells were transferred from the stock culture. To prevent nutrient contamination, all culture vessels and containers were cleaned by soaking in 1.2 M HCl for at least 24 h and rinsed with 18.2 MΩ cm Milli-Q water (Millipore; Bedford, MA, USA), followed by microwave sterilization. All stock solutions and media were prepared using high-purity analytical grade chemicals and freshly collected Milli-Q water. Acid-cleaned 250 mL polycarbonate bottles (Nalgene, USA) were used for stock solution preparation and storage to prevent iron contamination. Acid-cleaned 4 L polycarbonate bottles (Nalgene, USA) were used to prepare the culture media. 250 mL of each type of media were transferred into the 250 mL polycarbonate bottles and then put into a growth chamber under the experimental conditions overnight before use.

Chlorophyll and carotenoid measurements. Samples (7 mL) of culture were filtered onto Whatman GF/F membranes (effective pore size, ~0.7 µm) under gentle vacuum pressure (<18 kPa or 5 in Hg) and low-light, followed by an overnight extraction with 90% acetone in the dark at 4°C. Samples were then centrifuged at 4,300*g*, 4°C for 10 min. The absorption of the supernatant was measured at 480, 630, 664, and 750 nm using a UV-vis spectrophotometer (Shimadzu UV-2700). The Chl *a* content was calculated following Jeffrey and Humphrey (1975). Total Car content was calculated following Davies (1976).

Chlorophyll fluorescence measurements. The maximum quantum yield of PSII photochemistry (F$_v$/F$_m$) and the functional absorption cross-section of PSII (σ$_{PSII}$ with instrument-specific calibration factors (Satlantic)), were measured by a Fluorescence Induction and Relaxation System (FIRe, Satlantic, Halifax, Canada). Excitation was achieved using a high-luminosity blue (455 ± 20 nm) light-emitting diode (LED) array. PSII photochemistry parameters were determined by fitting the biophysical (KPF) model of Kolber et al. (1998) to each fluorescence transient using the FIREPRO 4.3 software provided by Satlantic. Twenty to 30 replicate measurements were made on a sample and averaged. The PSII operating efficiency

TABLE 1. Description of the experimental treatments used in this study.

Treatments	Time (h)	Media	Description	Temperature (°C)	Light intensity (μmol · m^{-2} · s^{-1})	pH
Control	0, 2, 6, 24, 72 h	ESAW	Full nutrients	20	100	8.1
N-starvation	0, 2, 6, 24, 72 h	N-free ESAW	No $NaNO_3$ addition	20	100	8.1
P-starvation	0, 2, 6, 24, 72 h	P-free ESAW	No Na_2PO_4 addition	20	100	8.1
Si-starvation	0, 2, 6, 24, 72 h	Si-free ESAW	No $Na_2SiO_3 \cdot 9H_2O$ addition	20	100	8.1
Fe-starvation	0, 2, 6, 24, 72 h	Fe-free ESAW	No $FeCl_3 \cdot 6H_2O$ addition, with 100 μM Na_2EDTA	20	100	8.1
ROS	0, 2, 6, 24, 72 h	ESAW	0.165 mM H_2O_2 addition	20	100	8.1
Low-temperature	0, 2, 6, 24, 72 h	ESAW	Full nutrients	14	100	8.1
High-temperature	0, 2, 6, 24, 72 h	ESAW	Full nutrients	26	100	8.1
Low-light	0, 2, 6, 24, 72 h	ESAW	Full nutrients	20	10	8.1
High-light	0, 2, 6, 24, 72 h	ESAW	Full nutrients	20	800	8.1
Low-pH	0, 2, 6, 24, 72 h	ESAW	Full nutrients	20	100	7.8

ESAW media was prepared according to Berges et al. 2001, but with some modifications. The nutrient-replete treatments and controls had final concentrations of 100 μM $NaNO_3$, 20 μM Na_2PO_4, 150 μM $Na_2SiO_3 \cdot 9H_2O$, and 6.56 μM Fe with a Na_2EDTA concentration of 100 μM. Nutrient starvation was induced by washing cells and then placing the cells in nutrient-free media. Temperature was maintained using growth chambers (Conviron A1000, Conviron, Manitoba, Canada). Continuous illumination was provided by LED bulbs. Irradiance was monitored using Biospherical Instruments QSL 2101. pH was set to pH 8.1 (control) or pH 7.8 (low-pH) using 16 mM N-(2-hydroxyethyl)-piperazine-N9-2-propanesulfonic acid (EPPS; Sigma-Aldrich), adjusted with ultra-pure HCl/NaOH. Time (h) refers to sampling time after initiation of treatment. All experiments were performed using four independent biological replicates.

under actinic light (Φ_{PSII}) and non-photochemical quenching (NPQ) was measured by a fast repetition rate fluorometry (FRRf) system using a PSI FL-3500 fluorometer and FluorWin software (Photon Systems Instruments, Drasov, Czech Republic). A train of 40 blue (455 nm, 30,000–85,000 μmol photons · m^{-2} · s^{-1}) flashlets with a duration of 1.2 μs separated by an intervening interval of 1.0 μs of darkness was used to progressively close PSII reaction centers and induce maximum fluorescence. After an initial measurement in the dark, an actinic light approximately equivalent to the growth light level (100 μmol photons · m^{-2}·s^{-1}, except for the low-light treatment: 8 μmol photons · m^{-2} · s^{-1} and high-light treatment: 800 μmol photons · m^{-2}·s^{-1}) was applied for 10 s following the protocols described by Liefer et al. (2018) and Xu et al. (2018). PSIWORX-R package (A. Barnett, sourceforge.net) were used to derive the following parameters: minimum fluorescence (F_0), maximum fluorescence (F_m), steady-state fluorescence at the growth irradiance (F_s), maximum fluorescence under actinic light equivalent to the growth irradiance (F_m'). Φ_{PSII} was calculated according to Genty et al. (1989), and NPQ was calculated according to Bilger and Björkman (1990) as follows:

$$\Phi_{PSII} = \left(F_m' - F_s'\right)/F_m' \tag{1}$$

$$NPQ = \left(F_m - F_m'\right)/F_m' \tag{2}$$

For both FIRe and FRRf measurements, two 2 mL samples were collected at each time point of the experiment and dark-adapted inside the incubator at their growth temperature for 15 min to ensure that the primary quinone-type acceptor was fully oxidized. Both measurements were made in a climate-controlled room at the same time.

Statistical analyses. All experiments were performed using four independent biological replicates. All data are presented as mean ± SD. A two-way ANOVA was used to determine if treatments and sampling times were associated with significant changes in each of the physiological parameters. To interpret the photophysiological parameters, we considered both the statistical difference (*t*-test, *P*-value < 0.05) and biological significance. Different photophysiolgical parameters exhibited very different orders of magnitude of variation in

response to the treatments; in particular NPQ was particularly sensitive. We therefore used a 40% change as a threshold to identify a treatment or time as having a biologically significant change on NPQ versus 5% change for all other parameters. Data analysis and visualizations, including a hierarchical clustering of the impact of each of the treatments on each physiological parameter, were conducted using the R v.3.6.1 (R Core Team 2019), packages ggplot2 v.3.2.0 (Wickham 2009), Pheatmap v.1.0.12 (Kolde 2019), and Factoextra v.1.0.5 (Kassambara and Mundt 2017).

RESULTS

The impact of all 10 stressors on accumulated growth, cell volume, pigment content and photophysiological parameters are expressed as a percent relative to the control (Figs. 1, 2) and as untransformed data (Table S1 in the Supporting Information). A two-way ANOVA (Table S2 in the Supporting Information) and heat maps (Fig. S1 in the Supporting Information) identify significant changes in physiology in response to the treatments and enable comparison of the relative magnitude and timing of these changes (Fig. 3, Fig. S1, Table S3 in the Supporting Information) across treatments and measured parameters. A principal component analysis illustrates how the stress treatments affect each observed parameter (Fig. 4).

Cell growth decreased or arrested under all environmental stresses tested except the high-temperature and low-pH treatments (Fig. 1a). Treatments form four clusters: rapid arrest of cell division, rapid but minor accelerated growth, rapid decreases and recovery in growth, and slower, gradual decreases in growth (Fig. S1). Si-starvation and H_2O_2 treatments form a cluster; both cause rapid cell division arrest. Under Si-starvation, growth was arrested by hour 2 (Fig. 3). The H_2O_2 treatment arrested growth by

hour 2, followed by recovery after 24 h. High-temperature and low-pH form a second cluster of a similar, short acceleration of growth within 24 h and 6 h respectively. A third cluster consists of the N-, P-, and Fe-starvation plus low-light and low-temperature treatments. Under N-, P-, and Fe-starvation, growth was initially similar to the control, then decreased sharply with turning points at 6 h (N-, Fe-starvation) and 24 h (P-starvation). Low-temperature and low-light both resulted in decreased growth rates. Under high light, cell growth ceased by 6 h but subsequently recovered.

Cell volume (μm^3) responses form four clusters: no decrease in cell volume (low-temperature, low-pH, and H_2O_2), small increases in cell volume, one treatment with a large increase in cell volume (Si-starvation), and two treatments that cause decreases in cell volume (Figs. 1b, S1). Fe-starvation had no effect on cell volume over the first 24 h, followed by an increase of 35% by 72 h. High-light increased cell volume rapidly (12% at 6 h but recovered to 8% at 72 h). P-starvation and high-temperature treatments causes increases in cell volume of 19% and 23% both at 72 h, but the increase under P-starvation was much faster (6 h) than under the high-temperature (24 h) treatment (Fig. 3a). Si-starvation led to a linear increase in cell volume starting after 2 h and caused the largest increase in cell volume observed of 135% after 72 h of Si-starvation. N-starvation and low light resulted in a decrease in cell volume by 16-19% (Fig. 3b), but the decrease under low light was much faster (onset at 2 h) than under N-starvation (onset at 6 h).

Intracellular Chl a concentration (fg · μm^{-3}) responses form three clusters: increases, moderate decreases, and large decreases. Intracellular Chl a concentration increased under low-light, high-temperature, and Si-starvation treatments (Figs. 1c, S1). Moderate decreases were caused by P-, Fe-starvation, low temperature, with very low decreases caused by low-pH and H_2O_2. The largest decreases were caused by N-starvation and high light. Total intracellular Car concentration generally increased relative to Chl a concentration resulting in an increase in the Car/Chl a under most treatments except for low-pH, low and high temperature and low light (Fig. 1d). The largest increases in Car/Chl a were in response to the N-starvation and the high-light treatment. Car/Chl a increased by almost 200% under N-starvation and approximately doubled under the high-light and Si-starvation treatments, with more moderate changes (33-71%) under P- and Fe-starvation and H_2O_2. The light, temperature, and H_2O_2 treatments led to low-magnitude changes but the most rapid increases in Car/Chl a.

Responses in F_v/F_m and the PSII operating efficiency under actinic light, Φ_{PSII} (Figs. 2, 3, S1) fall into four clusters. One cluster includes moderate increases (low-light) or no significant changes in PSII efficiency (low-pH and low-temperature treatments). The second and third clusters are characterized by

decreases under the nutrient starvation and high temperature. A fourth cluster includes the high-light and H_2O_2 treatments. The decreases are fastest and largest for N-, Si-starvation, H_2O_2, and high light. The responses to P- and Fe-starvation are slower by 72 h and have a larger magnitude effect than the light and temperature treatments. The Si-starvation and H_2O_2 treatments exhibited very similar decreases in F_v/F_m over the first 24 h of exposure, but diverged at 72 h with recovery in the H_2O_2 treatment and further changes in the Si-starvation treatment. The recovery process of the diatom in response to the H_2O_2 treatment reflects the decomposition of H_2O_2 over the time course of the experiment and the removal of H_2O_2 by cells (Pędziwiatr 2018), and an acclimation of the diatom to H_2O_2 damage.

Some patterns across treatments transcend the clusters. For Φ_{PSII}, there is an initial decrease at 0 h in response to the high-light treatment followed by a gradual and partial recovery and for low-light, an initial increase is followed by a partial recovery starting at 24 h. Temperature increase results in an initial increase in Φ_{PSII} for the first 12 h followed by a decrease from 24 to 72 h; the pattern is reversed for the low-temperature treatment. Responses to light changes are generally faster than changes in response to temperature, although the magnitudes are similar after 72 h. A similar, but slightly slower pattern for F_v/F_m is observed for these treatments. Generally, Φ_{PSII} changes more quickly and with larger magnitude changes compared with F_v/F_m in response to changes in irradiance and temperature (Fig. 2).

The stress response of the σ_{PSII}, forms three clusters: large and rapid decreases (high-light and Si-starvation), large increase with a gradual onset for N-starvation, and a moderate increase (low-light) or decreases for the remainder (Figs. 2c, S1). Changes generally happen very quickly (within 2 h), but the responses to the low-light treatment takes 72 h. The magnitude of change is largest for high light (−52%), followed by Si-, Fe-, and N-starvation. N-starvation is unusual in that the initial response is a decrease in σ_{PSII} at 2 h followed by the largest increase across treatments at 72 h (Fig. 3).

Responses in NPQ to treatments are generally fast (0-6 h) and large in magnitude (67-2500%), except for the low-pH treatment which does not change in NPQ and Fe-starvation which takes 24 h for a change to be detected (Fig. 2d). The largest changes in NPQ result from P-starvation. The fastest change arises in the high-light treatment (a large increase within minutes, recorded at 0 h). The low-light treatment is distinguished by the largest negative response in NPQ. Light, temperature, and H_2O_2 treatments perturb NPQ followed by a partial recovery (Table S3).

Principal component analysis (PCA) of the photophysiological data was used to analyze the effects of environmental stressors (Fig. 4). Some of the vectors for the variables were in close proximity to each
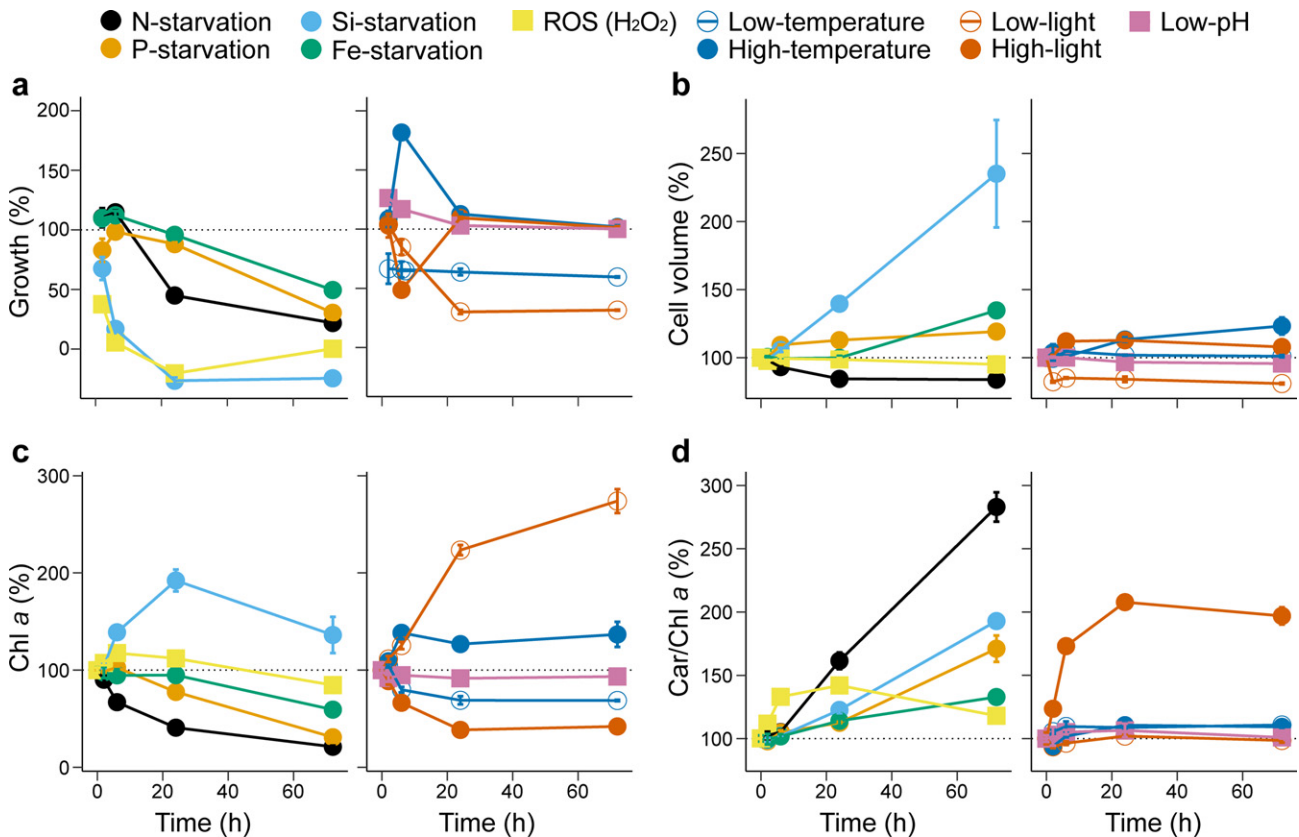
FIG. 1. Time-course response of growth (a), cell volume (μm^3) (b), intracellular Chl a concentration (fg · μm^{-3}) (c) and carotenoid (Car)/Chl a (d) of *Thalassiosira pseudonana* to 10 environmental stressors over 72 h. Growth (a) is the relative accumulated growth as defined in Materials and Methods (Growth, %). Treatments are divided across two panels (nutrient starvation and ROS (H_2O_2) on the left; temperature, light and pH treatments on the right). Data are plotted as percent relative to the control to facilitate comparison of the temporal trajectory and magnitude of change across measured parameters, with no change (100%) shown as a dotted line. The initial values of relative growth, cell volume, Chl a, and Car/Chl a at time 0 h are 0.00 ± 0.00, 58.75 ± 0.50 μm^3, 4.04 ± 0.11 fg·μm^{-3}, 0.23 ± 0.01, respectively. Values are means $\pm$ SD of four biological replicates. [Colour figure can be viewed at wileyonlinelibrary.com]

other: control, low-temperature, and low-pH (mostly moderate changes in photophysiology); N-, P- and Fe-starvation; and Si-starvation and H_2O_2, showing that the photophysiological parameters are affected similarity across treatments within each of these three groups of treatments. Vectors for Si-starvation and H_2O_2 are parallel indicating similarity in effects on photophysiology. The low-light vector is approximately the opposite direction as the high-light vector as might be expected from contrasting treatments. Unexpectedly, the Si-starvation vector is opposite to low-light and similar to the H_2O_2 and high-light vectors (due primarily to changes in cell volume and intracellular Chl a concentration). The high- and low-temperature vectors are in similar directions, indicating more similarity in response than contrasts for these treatments.

DISCUSSION

Marine phytoplankton are exposed to rapid changes in numerous environmental conditions that affect their ability to photosynthesize and

reproduce. Here, we identify: i) the most common photophysiological response to environmental stressors, and ii) potentially diagnostic differences in magnitude and timing of specific photophysiological parameters to particular environmental conditions in a model marine diatom. We build upon past work to improve our understanding of the relative impact of environmental stressors on the photophysiology of diatoms (Geider et al. 1993, Vassiliev et al. 1995, Parkhill et al. 2001, Young and Beardall 2003, Murata et al. 2007, Suggett et al. 2009, Liu et al. 2011, Tikkanen et al. 2014). A key strength of our experiments is the large number of stressful conditions examined on a single species in otherwise identical laboratory conditions, which enables comparison of the timing and magnitude of the stressful impacts on photophysiology. This synthesis is difficult to achieve from a comparative analysis of many independent experiments reported in the literature.

The common photophysiological stress response (PSR). In photoautotrophs, changing environmental conditions can lead to an imbalance between light acquisition and metabolic demand resulting in
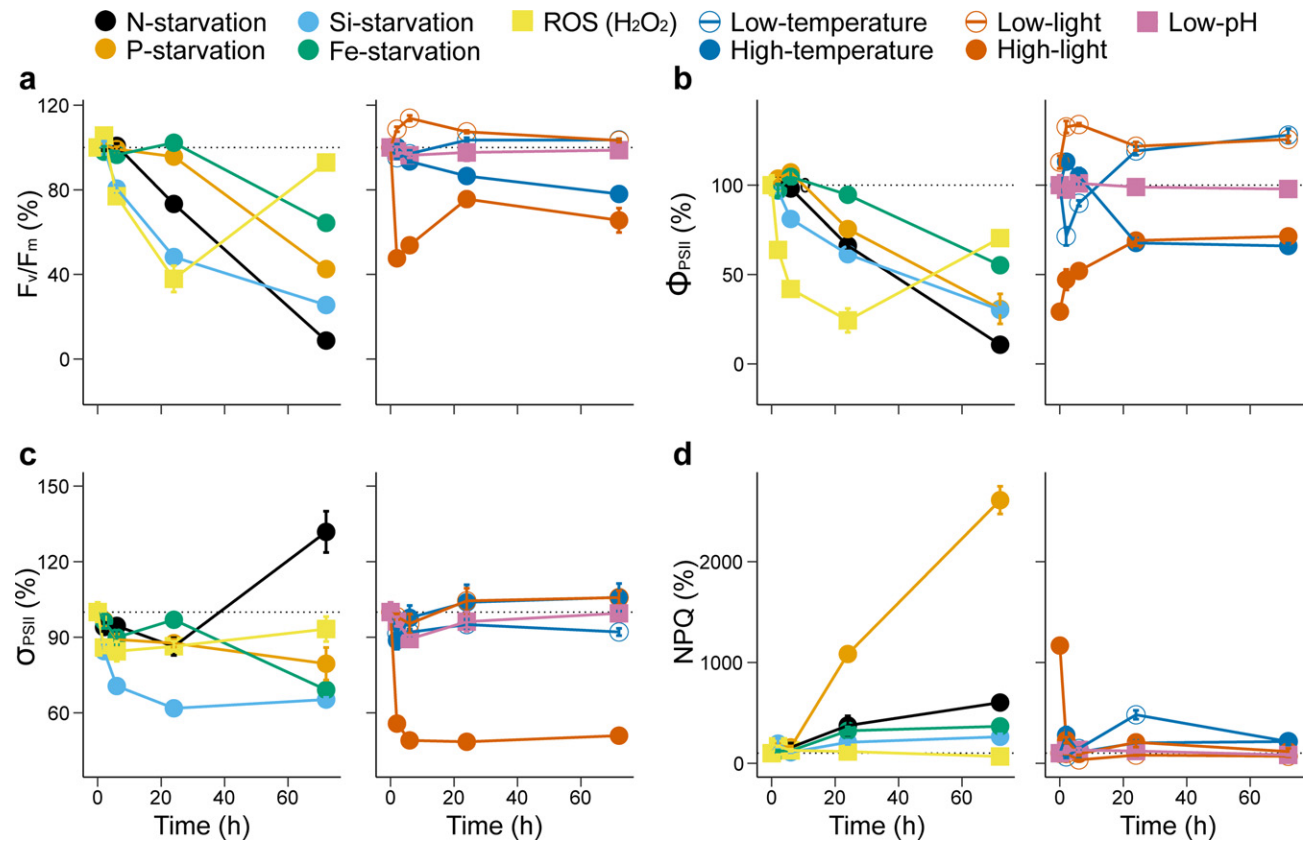
FIG. 2. Time course of the photosynthetic response of *Thalassiosira pseudonana* in response to 10 environmental stressors over 72 h. The maximum quantum yield of PSII photochemistry (F_v/F_m) (a), the PSII operating efficiency under actinic light (Φ_{PSII}) (b), the functional absorption cross-section of PSII (σ_{PSII}) (c), and non-photochemical quenching (NPQ) (d). Treatments are divided across two panels (nutrient starvation and ROS (H_2O_2) on the left; temperature, light, and pH treatments on the right). Data are plotted as percent relative to the control to facilitate comparison of the temporal trajectory and magnitude of change across measured parameters, with no change (100%) shown as a dotted line. The initial values of F_v/F_m, Φ_{PSII}, σ_{PSII}, and NPQ at time 0 h are 0.52 ± 0.01, 0.21 ± 0.01, 310.02 ± 11.94 ($\mathring{A}^2 \cdot quanta^{-1}$), 0.05 ± 0.01, respectively. Values are means ± SD of four biological replicates. [Colour figure can be viewed at wileyonline library.com]

physiological stress. Here, we assess and compare the effects of diverse environmental stressors including an exogenously imposed ROS achieved by H_2O_2 addition. In broad terms, nutrient starvation leads to an energy supply surplus relative to metabolic demand resulting in the following consequences: growth slows or arrests, cell size increases (although not for N-starvation), Car/Chl *a* increases, NPQ increases, and the σ_{PSII} and quantum yield of PSII (F_v/F_m and Φ_{PSII}) generally decreases. These results are generally consistent with previous work on a variety of phytoplankton species exposed to both steady-state and transient nutrient stress (Young and Beardall 2003, Allen et al. 2008, Shemi et al. 2016, Smith et al. 2016, Cui et al. 2017). Decreases in σ_{PSII}, F_v/F_m and Φ_{PSII} act to reduce energy input while increases in Car and NPQ increase thermal dissipation of absorbed energy. Increasing light and decreasing temperature can similarly stimulate surplus energy supply relative to metabolic demand (Huner et al. 1998), and thus similarly results in decreases in Chl *a* and σ_{PSII} (to decrease energy influx), and increases in both Car/Chl *a* and NPQ

(to increase energy outflux). The ROS treatment stimulated transient responses in σ_{PSII}, F_v/F_m and Φ_{PSII} similar to many of the stressors that cause an energy surplus, suggesting many stressors cause photo-oxidative damage (Demmig-Adams and Adams 1992, Li et al. 2009). By contrast, the low-light and elevated temperature treatments cause an energy supply deficit relative to metabolic demand, resulting in an increase in Chl *a* to boost energy capture. Our decreased pH treatment had relatively mild consequences for cell physiology, similar to previous work (Hinga 2002, Crawfurd et al. 2011).

Diagnostic photophysiological responses for specific environmental stressors: nutrients. Although a common PSR can be identified for *Thalassiosira pseudonana*, there are anomalies in magnitude and temporal patterns in parameters that suggest we may be able to identify diagnostics for specific stressors. For example, across the nutrient treatments (N, P, Fe, Si), N-starvation tends to have the largest and fastest influence on F_v/F_m and Φ_{PSII}, followed by P-starvation and then Fe-starvation, likely due to differences in storage capacity for the different nutrients and the

a — Timing of change

Stressor	Growth	Cell volume	Chl a	Car/Chl a	F_v/F_m	Φ_{PSII}	σ_{PSII}	NPQ
N-starvation	6	6	2	24	24	24	2	2
P-starvation	24	6	24	24	72	6	6	2
Si-starvation	2	6	6	24	6	6	2	2
Fe-starvation	6	72	72	24	72	24	6	24
ROS (H_2O_2)	2		2	2	2	2	2	2
Low-temperature	2		6	2		2	2	6
High-temperature	6	24	2	2	6	2	2	2
Low-light	6	2	2	2	2	0	72	6
High-light	6	6	2	2	2	0	2	0
Low-pH	2		2				6	

no change — 0h — 2h — 6h — 24h — 72h

b — % change

Stressor	Growth	Cell volume	Chl a	Car/Chl a	F_v/F_m	Φ_{PSII}	σ_{PSII}	NPQ
N-starvation	14.7 / −78.2	−16.2	−78.9	183.0	−91.3	−89.2	−13.7 / 31.8	502.5
P-starvation	−69.70	19.2	−69.0	70.9	−57.5	7.2 / −69.2	−20.5	2510.7
Si-starvation	−126.60	135.1	92.2	92.8	−74.5	−69.8	−38.2	162.6
Fe-starvation	12.1 / −50.5	34.7	−40.6	32.9	−35.6	−44.8	−30.9	266.4
ROS (H_2O_2)	−120.50	0	17.5 / −15.4	42.1	5.7 / −62.1	−75.6	−15.5	69.0
Low-temperature	−40.40	0	−31.3	10.8	0	−28.2 / 28.0	−8.4	380.9
High-temperature	81.70	23.3	38.4	−5.9 / 10.7	−22.0	13.1 / −34.0	−11.2	179.1
Low-light	−70.00	−19.0	173.9	−6.3	13.8	33.9	5.8	−66.6
High-light	−51.4 / 9.5	12.8	−61.5	108.0	−52.4	−70.8	−51.5	1067.9
Low-pH	26.30	0	−8.4	0	0	0	−10.7	0

decreased and then increased
increased and then decreased
≤−100 −50 0 50 ≥100 %

FIG. 3. Heatmaps of the timing of change (a) and % change (b) of the largest changes in 8 physiological parameters across 10 environmental stressors over 72 h. In panel (a), timing of change is the shortest time (in h, numbers, and colors) required to observe a significant change (*t*-test, $P < 0.05$) above a threshold (see Materials and Methods) in the corresponding parameter. In panel (b), % change refers to the largest significant % increases and decreases in observed parameters (%, *t*-test, $P < 0.05$, numbers and colors) greater than a threshold over all time relative to control. Rapid changes to slower changes are highlighted in a gradient color of light brown to dark brown. Increases are highlighted in shades of brown and decreases in shades of green. The physiological parameters are growth (relative accumulated growth, defined in Materials and Methods), cell volume (μm^3), Chl *a* (fg · μm^{-3}), carotenoid (Car/Chl *a*), the maximum quantum yield of PSII photochemistry (F_v/F_m), the PSII operating efficiency under actinic light (Φ_{PSII}), the functional absorption cross-section of PSII (σ_{PSII}), and non-photochemical quenching (NPQ). [Colour figure can be viewed at wileyonlinelibrary.com]
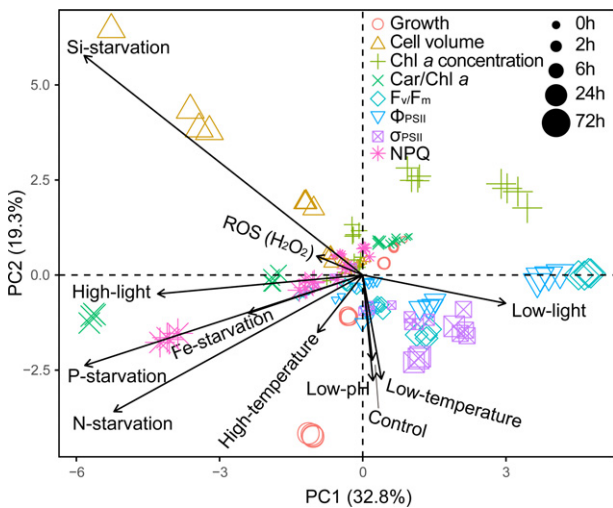
FIG. 4. Principal component analysis of physiological data across parameters and time in response to stress treatments. Each symbol corresponds to a particular parameter (color, shape) and time (size, smallest symbol at $t = 0$ h and largest symbol at $t = 72$ h). Loadings of each treatment on the first two principal component axes are shown as arrows. The first two principal components account for 52.1% of the total variance (PC1, 32.8% and PC2, 19.3%). The physiological parameters are growth (relative accumulated growth, defined in Materials and Methods), cell volume (μm^3), Chl *a* (fg · μm^{-3}), carotenoid (Car/Chl *a*), the maximum quantum yield of PSII photochemistry (F_v/F_m), the PSII operating efficiency under actinic light (Φ_{PSII}), the functional absorption cross-section of PSII (σ_{PSII}), and non-photochemical quenching (NPQ). [Colour figure can be viewed at wileyonlinelibrary.com]

relative requirements for these elements for growth and repair (Kilham et al. 1977, Tantanasarit et al. 2013). Protein and Chl are N-rich compounds. A lack of nitrogen rapidly reduces or arrests Chl biosynthesis and the ability to repair damaged PSII (Young and Beardall 2003, Tikkanen et al. 2014) resulting in rapid and large decreases in Chl concentration and decreases in F_v/F_m (Lavaud et al. 2016). N-starvation is unique among the nutrient stressors in causing a decrease in cell volume (protein is a large proportion of cell mass) and an increase in σ_{PSII} (31% after 72 h) likely caused by a reduction in the pigment packaging effect due to a large relative decrease in PSII antennae size relative to PSII reaction centers as has been observed in *Dunaliella* in response to Fe-starvation (Vassiliev et al. 1995). P-starvation led to rapid and very large increases in NPQ (2500%). Elevated NPQ is a common response to energy surplus, reflecting the dissipation capability of the organism (Müller et al. 2001). The enormous increase in NPQ in response to P-starvation suggests that NPQ plays a pivotal role in how diatoms respond to P-starvation and photo-oxidative damage. Phosphorus and energy metabolism are coupled through essential metabolites such as ATP and NADPH (Falkowski and Raven 2007). Consequently, a successful response to P-starvation may require rapid and strict regulation of energy and carbon metabolism (Brembu et al. 2017). Si-starvation led to the largest increases in cell volume

(135%) and one of the largest increases in Chl a (92%). In diatoms, Si is required to build the frustule and insufficient Si is known to arrest the cell cycle, leading to increases in cell volume (Booth and Harrison 1979, Martin-Jézéquel et al. 2000). The increase in Chl a during Si-starvation and consequent increases in energy supply may be compensated by decreases in F_v/F_m, Φ_{PSII}, and σ_{PSII}. Diatoms significantly increase their sinking rates when cells become bigger, under high irradiance, and under Si-starvation (Bienfang et al. 1982, Waite et al. 1997), therefore, the increase in cell volume under Si-starvation may facilitate a more rapid sinking out of stressful, high-light environments and relieve photo-oxidative stress. Compared to the other nutrient starvation treatments, Fe-starvation had a slower and more modest impact on the photophysiological parameters assayed. Fe stress has been reported to result in decreases in cell size, in contrast to our findings of increased cell size. This may be due to differences in response to transient versus steady-state Fe limitation (Sunda and Huntsman 1997, Leynaert et al. 2004, Allen et al. 2008).

Diagnostic photophysiological responses for specific environmental stressors: light and temperature. Consistent with previous work (Sobrino and Neale 2007, Xu et al. 2017), we find *Thalassiosira pseudonana* can rapidly adjust its physiology to rebalance energy and metabolism in response to changing light and temperature (Fig. 3). Although some similarity in response is expected between the high-light and low-temperature treatments because these treatments both cause a light energy surplus relative to metabolic demand and between the low-light and high-temperature treatments because they cause a light energy deficit relative to metabolic demand (Huner et al. 1998), there are more differences than similarities in the parameters (Fig. 4). In terms of similarities, both the low-temperature and high-irradiance treatments stimulated an immediate (<2 h) decrease in Φ_{PSII}, followed by partial recovery to about −30% of the control under the high-light treatment and about + 30% of the control under the low-temperature treatment, indicating rapid remodeling of the PSII reaction centers under these stressors. High-light is associated with photoinhibition of F_v/F_m and Φ_{PSII} and a fast, high-magnitude induction of NPQ (~10-fold higher than under low-temperature). However, after 2 h, as the cell acclimates, NPQ relaxes to a level comparable to many other stressors, including low temperature. Low temperature has no direct effect on the photon dose or direct photoinhibition, but likely reduces PSII repair and de novo PSII protein synthesis (Murata et al. 2007). Unlike most of the other stressors, low temperature did not stimulate an increase in Car/Chl a, indicating NPQ is the dominant mechanism used by *T. pseudonana* to respond to low temperature. Low light differs from other stressors in causing a moderate increase in σ_{PSII}, an increase in F_v/F_m and Φ_{PSII}, and a decrease

in NPQ (Li and Campbell 2017, Xu et al. 2017), and the largest increases in Chl a and Car and the largest decreases in cell volume. In aggregate these changes increase the efficiency of light harvesting and quantum yield. There is no similarity in photophysiological response between the low-light and high-temperature treatments, except both Chl a, Car, and Φ_{PSII} increase, perhaps facilitating increased light capture and quantum efficiency to fuel metabolic demand (Brooks and Farquhar 1985, Gillooly et al. 2001, Hancke and Glud 2004). It is worth noting that although the elevated temperature here is above its published growth optimum (Boyd et al. 2013), it significantly accelerated the growth rate at 6 h in this study.

The importance of timing. Some photophysiological parameters are inherently more difficult to interpret due to their dynamic responses to environmental stressors. Photophysiological responses synthesize the direct impact of the stressor on the cell, photoacclimation and metabolic remodelling, accumulated cellular damage, and changes in repair capacity. These processes operate at different rates and may lead to a lag followed by sustained unidirectional change in physiological performance or a saturating response, or a short-term perturbation followed by recovery. Changes in conditions (temperature, light, ROS) tend to stimulate the most rapid changes in photophysiology and are most likely to result in a perturbation and recovery trajectory, compared to nutrient starvation (Figs. 1-3). One example is the very large induction of NPQ (>1000%) at the initiation of the high-light treatment (<2 h) followed by recovery by 72 h. A more complex example is the rapid increase in Φ_{PSII} at 2 h followed by a rapid decrease over the next 22 h in response to low light. In contrast, in the low-temperature treatment Φ_{PSII} decreases rapidly over the first 2 h and then increases over the next 18 h. The variety in rates of responses to stressors (Figs. 1-3) and especially the perturbation and recovery can make observations of fluorescence responses made at a single time point from a dynamic field site challenging. Parameters can both increase and then decrease, or decrease and then increase, relative to the control over time. Our experiments provide guidance on the relative rates and responses which can be anticipated across stressors.

CONCLUSIONS

Resource starvation, shifts in light and temperature induce an array of photophysiolgoical responses to changes in light acquisition, metabolic demand and imbalance, and altered rates of damage and repair of cellular machinery. *Thalassiosira pseudonana* exhibits a common photophysiolgical stress response (PSR) to many stressors: cell division slows/arrests, cell volume increases, Chl a declines, Car/Chl a increases, the cross-section and efficiency

of PSII declines, and NPQ increases. Some diagnostic differences in the PSR for particular nutrient stressors include a large decrease in cell volume and an increase in σ_{PSII} after 24 h of N-starvation; a large increase in NPQ after> 24-72 h of P-starvation; and very large increases in cell volume and Chl *a*, and decreases in σ_{PSII} under Si-starvation. Changes in conditions, irradiance and temperature cause a variety of relatively rapid and transient responses, for example, a large, rapid increase in NPQ with initial exposure to high-light and rapid decline in Φ_{PSII} followed by recovery under both high light and low temperature. The low-light and low-temperature treatments uniquely stimulate an increase in PSII quantum efficiency. Future work is required to investigate how interactions among stressors alter photophysiological responses and the generality of these results to other diatoms and phytoplankton taxa from other evolutionary lineages.

Abida, H., Dolch, L. J., Meï, C., Villanova, V., Conte, M., Block, M. A., Finazzi, G., Bastien, O., Tirichine, L. & Bowler, C. 2015. Membrane glycerolipid remodeling triggered by nitrogen and phosphorus starvation in *Phaeodactylum tricornutum*. *Plant Physiol.* 167:118–36.

Alipanah, L., Rohloff, J., Winge, P., Bones, A. M. & Brembu, T. 2015. Whole-cell response to nitrogen deprivation in the diatom *Phaeodactylum tricornutum*. *J. Exp. Bot.* 66:6281–96.

Alipanah, L., Winge, P., Rohloff, J., Najafi, J., Brembu, T. & Bones, A. M. 2018. Molecular adaptations to phosphorus deprivation and comparison with nitrogen deprivation responses in the diatom *Phaeodactylum tricornutum*. *PLoS ONE* 13:e0193335.

Allen, A. E., LaRoche, J., Maheswari, U., Lommer, M., Schauer, N., Lopez, P. J., Finazzi, G., Fernie, A. R. & Bowler, C. 2008. Whole-cell response of the pennate diatom *Phaeodactylum tricornutum* to iron starvation. *Proc. Natl. Acad. Sci. USA* 105:10438–43.

Armbrust, E. V. 2009. The life of diatoms in the world's oceans. *Nature* 459:185–92.

Behrenfeld, M. J., Worthington, K., Sherrell, R. M., Chavez, F. P., Strutton, P., McPhaden, M. & Shea, D. M. 2006. Controls on tropical Pacific Ocean productivity revealed through nutrient stress diagnostics. *Nature* 442:1025–8.

Berges, J. A., Franklin, D. J. & Harrison, P. J. 2001. Evolution of an artificial seawater medium: improvements in enriched seawater, artificial water over the last two decades. *J. Phycol.* 37:1138–45.

Bienfang, P. K., Harrison, P. J. & Quarmby, L. M. 1982. Sinking rate response to depletion of nitrate, phosphate and silicate in four marine diatoms. *Mar. Biol.* 67:295–302.

Bilger, W. & Björkman, O. 1990. Role of the xanthophyll cycle in photoprotection elucidated by measurements of light-induced absorbance changes, fluorescence and photosynthesis in leaves of *Hedera canariensis*. *Photosynth. Res.* 25:173–85.

Booth, B. & Harrison, P. J. 1979. Effect of silicate limitation on valve morphology in *Thalassiosira* and *Coscinodiscus* (Bacillariophyceae). *J. Phycol.* 15:326–9.

Boyd, P. W. & Abraham, E. R. 2001. Iron-mediated changes in phytoplankton photosynthetic competence during SOIREE. *Deep-Sea Res. Part II Top. Stud. Oceanogr.* 48:2529–50.

Boyd, P. W., Collins, S., Dupont, S., Fabricius, K., Gattuso, J. P., Havenhand, J., Hutchins, D. A., et al. 2018. Experimental strategies to assess the biological ramifications of multiple drivers of global ocean change – a review. *Glob. Chang. Biol* 24:2239–61.

Boyd, P. W., Rynearson, T. A., Armstrong, E. A., Fu, F., Hayashi, K., Hu, Z., Hutchins, D. A., Kudela, R. M., Litchman, E. & Mulholland, M. R. 2013. Marine phytoplankton temperature versus growth responses from polar to tropical waters–outcome of a scientific community-wide study. *PLoS ONE* 8:e63091.

Brembu, T., Mühlroth, A., Alipanah, L. & Bones, A. M. 2017. The effects of phosphorus limitation on carbon metabolism in diatoms. *Philos. T. R. Soc. B* 372:20160406.

Brennan, G. & Collins, S. 2015. Growth responses of a green alga to multiple environmental drivers. *Nat. Clim. Change* 5:892–7.

Brooks, A. & Farquhar, G. D. 1985. Effect of temperature on the CO_2/O_2 specificity of ribulose-1, 5-bisphosphate carboxylase/oxygenase and the rate of respiration in the light. *Planta* 165:397–406.

Crawfurd, K. J., Raven, J. A., Wheeler, G. L., Baxter, E. J. & Joint, I. 2011. The response of *Thalassiosira pseudonana* to long-term exposure to increased CO_2 and decreased pH. *PLoS ONE* 6:e26695.

Cui, Y., Zhang, H. & Lin, S. 2017. Enhancement of non-photochemical quenching as an adaptive strategy under phosphorus deprivation in the dinoflagellate *Karlodinium veneficum*. *Front. Microbiol.* 8:404.

Davies, B. H. 1976. Chemistry and biochemistry of plant pigments. *Carotenoids* 2:38–165.

De La Rocha, C. L. & Passow, U. 2004. Recovery of *Thalassiosira weissflogii* from nitrogen and silicon starvation. *Limnol. Oceanogr.* 49:245–55.

Demmig-Adams, B. & Adams, W. W III. 1992. Photoprotection and other responses of plants to high light stress. *Annu. Rev. Plant Biol.* 43:599–626.

Falkowski, P. G. & Raven, J. A. 2007. *Aquatic photosynthesis*, 2nd ed. Princeton University Press, Princeton, New Jersey, 484 pp.

Field, C. B., Behrenfeld, M. J., Randerson, J. T. & Falkowski, P. 1998. Primary production of the biosphere: integrating terrestrial and oceanic components. *Science* 281:237–40.

Gao, K., Beardall, J., Häder, D. P., Hall-Spencer, J. M., Gao, G. & Hutchins, D. A. 2019. Effects of ocean acidification on marine photosynthetic organisms under the concurrent influences of warming, UV radiation and deoxygenation. *Front. Mar. Sci.* 6:322.

Geider, R. J., La Roche, J., Greene, R. M. & Olaizola, M. 1993. Response of the photosynthetic apparatus of *Phaeodactylum tricornutum* (Bacillariophyceae) to nitrate, phosphate, or iron starvation. *J. Phycol.* 29:755–66.

Genty, B., Briantais, J. M. & Baker, N. R. 1989. The relationship between the quantum yield of photosynthetic electron transport and quenching of chlorophyll fluorescence. *Biochim. Biophys. Acta Gen. Subj.* 990:87–92.

Gillooly, J. F., Brown, J. H., West, G. B., Savage, V. M. & Charnov, E. L. 2001. Effects of size and temperature on metabolic rate. *Science* 293:2248–51.

Gorbunov, M. Y. & Falkowski, P. G. 2005. Fluorescence induction and relaxation (FIRe) technique and instrumentation for monitoring photosynthetic processes and primary production in aquatic ecosystems. *Proc. 13th International Congress of Photosynthesis. In* van der Est, A. & Bruce, D. [Eds.]. Allen Press, Montreal, Quebec, pp. 1029–31.

Hancke, K. & Glud, R. N. 2004. Temperature effects on respiration and photosynthesis in three diatom-dominated benthic communities. *Aquat. Microb. Ecol.* 37:265–81.

Hinga, K. R. 2002. Effects of pH on coastal marine phytoplankton. *Mar. Ecol. Prog. Ser.* 238:281–300.

Hughes, D. J., Varkey, D., Doblin, M. A., Ingleton, T., Mcinnes, A., Ralph, P. J., van Dongen-Vogels, V. & Suggett, D. J. 2018. Impact of nitrogen availability upon the electron requirement for carbon fixation in Australian coastal phytoplankton communities. *Limnol. Oceanogr.* 63:1891–910.

Huner, N. P., Öquist, G. & Sarhan, F. 1998. Energy balance and acclimation to light and cold. *Trends Plant Sci.* 3:224–30.

Jeffrey, S. W. & Humphrey, G. F. 1975. New spectrophotometric equations for determining chlorophylls a, b, c1 and c2 in higher plants, algae and natural phytoplankton. *Biochem. Physiol. Pflanz.* 167:191–4.

Kassambara, A. & Mundt, F. 2017. Factoextra: extract and visualize the results of multivariate data analyses. R package version 1.0.5. [WWW document] https://CRAN.R-project.org/package=factoextra [accessed Jan 2020].

Kilham, S. S., Kott, C. L. & Tilman, D. 1977. Phosphate and silicate kinetics for the Lake Michigan diatom *Diatoma elongatum*. *J. Great Lakes Res.* 3:93–9.

Kolber, Z. S., Prášil, O. & Falkowski, P. G. 1998. Measurements of variable chlorophyll fluorescence using fast repetition rate techniques: defining methodology and experimental protocols. *Biochim. Biophys. Acta Bioenerg.* 1367:88–106.

Kolde, R. 2019. Pheatmap: Pretty Heatmaps. R package version 1.0.12. [WWW document] https://CRAN.R-project.org/package=pheatmap [accessed Jan 2020].

Kramer, D. M. & Evans, J. R. 2011. The importance of energy balance in improving photosynthetic productivity. *Plant Physiol.* 155:70–8.

Lavaud, J., Six, C. & Campbell, D. A. 2016. Photosystem II repair in marine diatoms with contrasting photophysiologies. *Photosynth. Res.* 127:189–99.

Leynaert, A., Bucciarelli, E., Claquin, P., Dugdale, R. C., Martin-Jézéquel, V., Pondaven, P. & Ragueneau, O. 2004. Effect of iron deficiency on diatom cell size and silicic acid uptake kinetics. *Limnol. Oceanogr.* 49:1134–43.

Li, F., Beardall, J. & Gao, K. 2018. Diatom performance in a future ocean: interactions between nitrogen limitation, temperature, and CO_2-induced seawater acidification. *ICES J. Mar. Sci.* 75:1451–64.

Li, G. & Campbell, D. A. 2017. Interactive effects of nitrogen and light on growth rates and RuBisCO content of small and large centric diatoms. *Photosynth. Res.* 131:93–103.

Li, Z., Wakao, S., Fischer, B. B. & Niyogi, K. K. 2009. Sensing and responding to excess light. *Annu. Rev. Plant Biol.* 60:239–60.

Liefer, J. D., Garg, A., Campbell, D. A., Irwin, A. J. & Finkel, Z. V. 2018. Nitrogen starvation induces distinct photosynthetic responses and recovery dynamics in diatoms and prasinophytes. *PLoS ONE* 13:e0195705.

Liu, S., Guo, Z., Li, T., Huang, H. & Lin, S. 2011. Photosynthetic efficiency, cell volume, and elemental stoichiometric ratios in *Thalassirosira weissflogii* under phosphorus limitation. *Chin. J. Oceanol. Limnol.* 29:1048–56.

Martin-Jézéquel, V., Hildebrand, M. & Brzezinski, M. A. 2000. Silicon metabolism in diatoms: implications for growth. *J. Phycol.* 36:821–40.

Moore, C. M., Suggett, D. J., Hickman, A. E., Kim, Y. N., Tweddle, J. F., Sharples, J., Geider, R. J. & Holligan, P. M. 2006. Phytoplankton photoacclimation and photoadaptation in response to environmental gradients in a shelf sea. *Limnol. Oceanogr.* 51:936–49.

Müller, P., Li, X. P. & Niyogi, K. K. 2001. Non-photochemical quenching. A response to excess light energy. *Plant Physiol.* 125:1558–66.

Murata, N., Takahashi, S., Nishiyama, Y. & Allakhverdiev, S. I. 2007. Photoinhibition of photosystem II under environmental stress. *Biochim. Biophys. Acta BBA-Bioenerg.* 1767:414–21.

Parkhill, J. P., Maillet, G. & Cullen, J. J. 2001. Fluorescence-based maximal quantum yield for PSII as a diagnostic of nutrient stress. *J. Phycol.* 37:517–29.

Pędziwiatr, P. 2018. Decomposition of hydrogen peroxide-kinetics and review of chosen catalysts. *Acta Innovations* 26:45–52.

Prasil, O., Suggett, D. J., Cullen, J. J. & Babin, M. 2008. Aquafluo 2007: chlorophyll fluorescence in aquatic sciences, an international conference held in Nové Hrady. *Photosynth. Res.* 95:111–5.

R Core Team. 2019. *R: A language and environment for statistical computing. Version 3.6.1.* R Foundation for Statistical Computing. Vienna, Austria. [WWW document] URL http://www.R-project.org/ [accessed July 2019].

Shemi, A., Schatz, D., Fredricks, H. F., Van Mooy, B. A., Porat, Z. & Vardi, A. 2016. Phosphorus starvation induces membrane remodeling and recycling in *Emiliania huxleyi*. *New Phytol.* 211:886–98.

Smith, S. R., Glé, C., Abbriano, R. M., Traller, J. C., Davis, A., Trentacoste, E., Vernet, M., Allen, A. E. & Hildebrand, M. 2016. Transcript level coordination of carbon pathways during silicon starvation-induced lipid accumulation in the diatom *Thalassiosira pseudonana*. *New Phytol.* 210:890–904.

Sobrino, C. & Neale, P. J. 2007. Short-term and long-term effects of temperature on photosynthesis in the diatom *Thalassiosira pseudonana* under UVR exposures. *J. Phycol.* 43:426–36.

Suggett, D. J., Moore, C. M., Hickman, A. E. & Geider, R. J. 2009. Interpretation of fast repetition rate (FRR) fluorescence: signatures of phytoplankton community structure versus physiological state. *Mar. Ecol. Prog. Ser.* 376:1–19.

Sunda, W. G. & Huntsman, S. A. 1997. Interrelated influence of iron, light and cell size on marine phytoplankton growth. *Nature* 390:389–92.

Tantanasarit, C., Englande, A. J. & Babel, S. 2013. Nitrogen, phosphorus and silicon uptake kinetics by marine diatom *Chaetoceros calcitrans* under high nutrient concentrations. *J. Exp. Mar. Biol. Ecol.* 446:67–75.

Tikkanen, M., Mekala, N. R. & Aro, E. M. 2014. Photosystem II photoinhibition-repair cycle protects Photosystem I from irreversible damage. *Biochim. Biophys. Acta BBA-Bioenerg.* 1837:210–5.

Tréguer, P., Bowler, C., Moriceau, B., Dutkiewicz, S., Gehlen, M., Aumont, O., Bittner, L., Dugdale, R., Finkel, Z. & Iudicone, D. 2018. Influence of diatom diversity on the ocean biological carbon pump. *Nat. Geosci.* 11:27–37.

Vassiliev, I. R., Kolber, Z., Wyman, K. D., Mauzerall, D., Shukla, V. K. & Falkowski, P. G. 1995. Effects of iron limitation on photosystem II composition and light utilization in *Dunaliella tertiolecta*. *Plant Physiol.* 109:963–72.

Waite, A., Fisher, A., Thompson, P. A. & Harrison, P. J. 1997. Sinking rate versus cell volume relationships illuminate sinking rate control mechanisms in marine diatoms. *Mar. Ecol. Prog. Ser.* 157:97–108.

Wickham, H. 2009. *ggplot2: elegant graphics for data analysis.* Springer, New York, NY, USA.

Wilson, K. E., Ivanov, A. G., Öquist, G., Grodzinski, B., Sarhan, F. & Huner, N. P. 2006. Energy balance, organellar redox status, and acclimation to environmental stress. *Botany* 84:1355–70.

Xu, K., Grant-Burt, J. L., Donaher, N. & Campbell, D. A. 2017. Connectivity among Photosystem II centers in phytoplankters: Patterns and responses. *Biochim. Biophys. Acta BBA-Bioenerg.* 1858:459–74.

Xu, K., Lavaud, J., Perkins, R., Austen, E., Bonnanfant, M. & Campbell, D. A. 2018. Phytoplankton σ_{PSII} and excitation dissipation; implications for estimates of primary productivity. *Front. Mar. Sci.* 5:281.

Young, E. B. & Beardall, J. 2003. Photosynthetic function in *Dunaliella tertiolecta* (Chlorophyta) during a nitrogen starvation and recovery cycle. *J. Phycol.* 39:897–905.

Supporting Information

Additional Supporting Information may be found in the online version of this article at the publisher's web site:

Figure S1. Heatmap and hierarchical clustering of physiological parameters as a function of 10 environmental stressors over 72 h.

Table S1. Experimental data from the control and 10 stress treatments for each observed physiological parameter.

Table S2. Two-way ANOVA of the effects of treatment and time on the different physiological variables.

Table S3. Average percent change in physiological parameters as a function of 10 environmental stressors over 72 h.